scientific reports

Check for updates

OPEN

Amplified quantum battery via dynamical modulation

Maryam Hadipour[1], Negar Nikdel Yousefi[2], Ali Mortezapour[3], Amir Sharifi Miavaghi[1] & Soroush Haseli[1,4]✉

We investigate the charging dynamics of a frequency-modulated quantum battery (QB) placed within a dissipative cavity environment. Our study focuses on the interaction of such a battery under both weak and strong coupling regimes, employing a model in which the quantum battery and charger are represented as frequency-modulated qubits indirectly coupled through a zero-temperature environment. It is demonstrated that both the modulation frequency and amplitude are crucial for optimizing the charging process and the ergotropy of the quantum battery. Specifically, high-amplitude, low-frequency modulation significantly enhances charging performance and work extraction in the strong coupling regime. As an intriguing result, it is deduced that modulation at very low frequencies leads to the emergence of energy storage and work extraction in the weak coupling regime. Such a result can never be achieved without modulation in the weak coupling regime. These results highlight the importance of adjusting modulation parameters to optimize the performance of quantum batteries for real-world applications in quantum technologies.

Keywords Ergotropy, Non-equilibrium, Quantum coherence

Every quantum system is inherently open to interactions with its environment. These inevitable interactions can result in the loss of crucial quantum properties such as entanglement, coherence, and system energy disturbances[1]. The preservation of these quantum properties for efficient energy storage is a key area of study in the theory of open quantum systems. Therefore, it's vital to consider the dissipative effects of the environment during the charging process of quantum batteries (QBs). This understanding necessitates the study of quantum batteries within the framework of open quantum systems[2–54]. QBs are d-dimensional quantum systems with non-degenerate energy levels. These devices are used to storage of energy in quantum degrees of freedom for facilitating the transfer of energy from production to consumption hubs. A desirable quantum battery should possess two important features: firstly, it should be optimally charged within a short period of time, and secondly, its stored energy should be fully utilized at consumption centers, or in other words, the extraction of work form QBs should occur optimally. Hence, establishing the conditions to attain these two crucial characteristics for quantum batteries is of significant importance. Recent studies in the field of QBs have concentrated on scenarios of open systems, where the battery and charger in contact with the environment[3–8,11,12].

Recent advancements in quantum energy storage and battery technologies have opened new possibilities in the field, with a particular emphasis on leveraging quantum effects for enhancing performance. One of the critical developments has been the application of collisional models in understanding the interactions between quantum systems and their environments, especially regarding energy transfer. In Ref.[49], the authors show that the charging dynamics of a quantum battery, modeled via a collisional framework, are strongly influenced by non-Markovian effects. They demonstrate that the maximum steady-state ergotropy can be reached either in a memoryless environment in the large-loss limit or in a memory-affected environment beyond this limit. Notably, environments with memory enable near-optimal ergotropy across a broader parameter space and potentially in shorter times. Interestingly, the ergotropy maximum corresponds to zero non-Markovianity, suggesting a subtle interplay between memory effects induced by the environment and those introduced by the charger. In Ref.[55], the authors show that collective quantum resources can significantly enhance the charging power of quantum batteries composed of many identical units. They study a model consisting of N two-level systems coupled to a common photonic mode in a cavity (the "Dicke QB") and compare it to a configuration where each two-level system interacts with its own cavity mode (the "Rabi QB"). Using exact diagonalization, they demonstrate that the Dicke QB exhibits a genuine quantum advantage in charging power, scaling as $\sqrt{N}$ for large N due to entanglement generated by the shared photonic mode. In Ref.[56], the authors show that energy dissipation can be

[1]Faculty of Physics, Urmia University of Technology, Urmia, Iran. [2]Quantum Technologies Research Center (QTRC), Science and Research Branch, Islamic Azad University, Tehran, Iran. [3]Department of Physics, University of Guilan, 41335-1914 Rasht, Iran. [4]School of Quantum Physics and Matter, Institute for Research in Fundamental Sciences (IPM), P.O. 19395-5531, Tehran, Iran. ✉email: soroush.haseli@uut.ac.ir

used as a resource to optimize quantum battery performance. They propose a charging method where coherent charger-battery interaction is replaced by a dissipative interaction via an engineered shared reservoir. This approach enhances energy redistribution and charging efficiency. The study highlights the role of detuning in the shared environment and its implications for quantum circuit battery architectures, offering practical justification for super-optimal charger-battery configurations. In Ref.[57], the authors show that a micromaser serves as an effective quantum battery model, achieving a steady state in the ultrastrong coupling regime. They also discuss the stability against qubit coherence loss and the impact of counter-rotating terms.

Motivated by these considerations, we aim to examine how frequency modulation can affect the dynamics of the charging process of QBs and work extraction from it in a model in which the charger-battery model is represented via a two-frequency-modulated qubit system. Generally, a quantum system experiences frequency modulation when its energy levels are changed by external driving. Frequency modulation in an atomic qubit can be performed by applying an external off-resonant field[58,59]. On the other hand, frequency modulation is now possible in superconducting Josephson qubits (artificial atoms), which are the preferred building blocks of contemporary quantum computer prototypes[60], thanks to recent experimental advancements in the fabrication and control of quantum circuit-QED devices[60–64]. It was shown that frequency modulation of a qubit could induce sideband transitions[65,66], modify its fluorescence spectrum[67], alter population dynamics[68–72], amplify non-Markovianity[73,74], quantum synchronization[75] and preserving quantum resources[74,76]. Furthermore, external control of the frequency of the qubit has facilitated the identification of an accurate relationship between non-Markovianity and quantum speed limit time (QSLT)[77].

Here, we focus on the scenario where the environment acts as a mediator between the QB and the charger. Indeed, this model allows for energy leakage from the battery into the environment, thereby facilitating a realistic situation of spontaneous discharge in quantum batteries. Our study adopts a model where a battery-charger system consists of two distinct frequency-modulated qubits interacting with a structured global environment. We consider both weak and strong coupling regimes in our model. This allows us to investigate how frequency modulation influences the charging process and work extraction across these regimes. The model we consider involves two distinct frequency-modulated qubits, the QB" and the charger," interacting with a global structured environment. We analyze this interaction to understand the dynamics and behavior of the charging and work extraction of the QB. The findings of our study could potentially be applied in the design and optimization of quantum battery systems. We observe a significant disruptive effect of the modulation mechanism when the resonance condition is present, against the optimal charging and work extraction from the quantum battery in both strong and weak coupling regimes. Furthermore, it is demonstrated that under non-resonant conditions, both the charging and the work extraction process of the QB can be carried out more optimally.

Ergotropy

Let us consider a scenario where the quantum battery (QB) is thermally insulated, preventing heat exchange with its surroundings. In this scenario, the work extraction process is cyclic, implying that the system returns to its initial Hamiltonian by the end of the process. The following unitary transformation can characterize this process[78]

$$U(t) = \exp\left[-i\int_0^t dt'(H_B + V(t'))\right]. \tag{1}$$

Where H_B is the Hamiltonian of the QB. $V(t')$ represents the time-dependent fields that extract energy from the quantum battery. In this paper, we have normalized the constant ($\hbar$) to 1 ($\hbar = 1$). Given that the process is cyclic, the field is zero at both the initial and final moments, i.e., $V(0) = V(t) = 0$. The work that can be extracted during this cyclic process is as follows[78]

$$W(\rho_B) = Tr(H_B\rho_B) - Tr(H_B U\rho_B U^\dagger), \tag{2}$$

in which ρ_B is the density matrix of the QB. By appropriately selecting $V(t')$, any unitary transformation U can be realized. Consequently, the maximum work that can be extracted from a quantum battery in a cyclic unitary process referred to as ergotropy, is determined by

$$\mathscr{W} = Tr(H_B\rho_B) - \min_U(H_B U\rho_B U^\dagger), \tag{3}$$

The minimization is computed over the ensemble of all attainable unitary transformations. It has been demonstrated that for any specified state ρ_B, there exists a singular state that optimizes the aforementioned relation. This state is referred to as the passive state[78]. So, the maximum amount of extractable work can be expressed as

$$\mathscr{W} = Tr(H_B\rho_B) - Tr(H_B\sigma_B), \tag{4}$$

where σ_B is the passive state associated with ρ_B. The passive state σ_B is characterized by a population distribution that decreases or remains constant concerning its Hamiltonian H_B, and it commutes with H_B, satisfying $[H_B, \sigma_B] = 0$. The spectral decomposition of the density matrix ρ_B and its associated Hamiltonian H_B can be expressed in the following form

$$\begin{aligned} \rho_B &= \sum_n r_n |r_n\rangle\langle r_n|, \quad r_1 \geq r_2 \geq \cdots \geq r_n \\ H_B &= \sum_m \varepsilon_m |\varepsilon_m\rangle\langle\varepsilon_m| \quad \varepsilon_1 \leq \varepsilon_2 \leq \cdots \leq \varepsilon_m, \end{aligned} \tag{5}$$

in which $r_n(|r_n\rangle)$ and $\varepsilon_m(|\varepsilon_m\rangle)$ are the eigenvalues (eigenstate) of the density matrix and Hamiltonian, respectively. Hence, the passive state σ_B can be written as[78]

$$\sigma_B = U\rho_B U^\dagger = \sum_i r_n |\varepsilon_n\rangle\langle\varepsilon_n|. \tag{6}$$

In general, by substituting Eqs. (5) and (6) into Eq. (4), the ergotropy can be obtained as[78]

$$\mathscr{W} = \sum_{mn} r_n \varepsilon_m \left(|\langle r_n|\varepsilon_m\rangle|^2 - \delta_{m,n} \right), \tag{7}$$

where $\delta_{m,n}$ is the Kronecker delta function.

Model

The model considered in this work consists of the QB (qubit B) and the charger (qubit A). Each qubit has ground and excited states, represented as $|g_j\rangle$ and $|e_j\rangle$ $(j = A, B)$, respectively. Both qubits are embedded in a high-Q cavity with quantized modes and are influenced by a zero-temperature environment, which acts as a mediator between the QB and the charger. The QB and charger are modulated sinusoidally by an external driving field. Modulating both the QB and the charger ensures that energy is coherently injected into the system in a symmetric and controllable manner. This facilitates resonant energy transfer and allows for a more efficient charging process, especially when the driving frequency matches the energy gaps of the modulated systems.. A schematic representation of the model is illustrated in Fig. 1.

The total Hamiltonian which describes the system consist of QB, charger and environment in the dipole and rotating wave approximations is given by[74]

$$H = H_0 + \mathscr{F}(t) H_I \tag{8}$$

$H_0 = H_A^m + H_B^m + H_E$, is the Hamiltonian of the total system, where $H_A^m + H_B^m$ describe the modulated two-qubit system and H_E represents the Hamiltonian of the environment. These components are given by[74]

$$\begin{aligned} H_j^m &= \frac{1}{2}[\omega_{0_j} + d_j \cos(\Omega_j t)]\sigma_z^j, \quad j \in \{A, B\} \\ H_E &= \sum_k \omega_k a_k^\dagger a_k. \end{aligned} \tag{9}$$

in the above expression, $\sigma_z^j = |e_j\rangle\langle e_j| - |g_j\rangle\langle g_j|$ represents the z-component of the Pauli operator for the jth qubit, which has a transition frequency ω_{0_j}. The variables d_j and Ω_j denote the amplitude and frequency of the modulation applied to the jth qubit, respectively. ω_k is the frequency of the quantized modes of the cavity, while

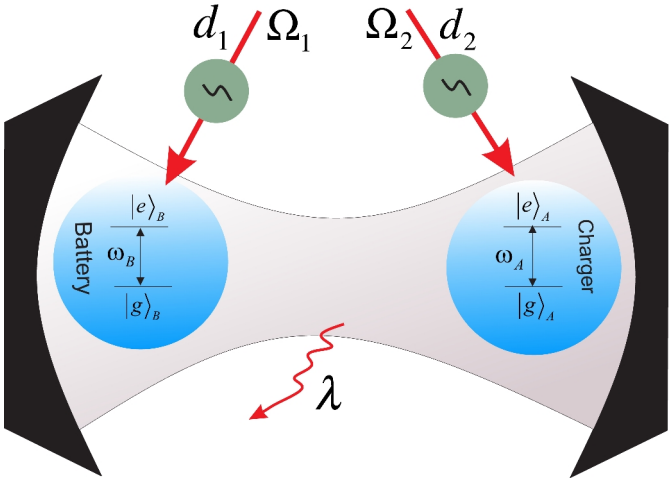

Fig. 1. Schematic representation of the model in which QB and charger (two frequency-modulated qubits) are embedded in a high-Q cavity.

a_k and $a_k^\dagger$ are the annihilation and creation operators for the kth mode of the cavity. In Eq. (8), H_I describes the interaction between the two qubits and the reservoir, which is expressed as follows:

$$H_I = H_{AE} + H_{BE} = \sum_k g_k \mu_1 \left(\sigma_{\mathrm{A}}^+ a_k + \sigma_{\mathrm{A}}^- a_k^\dagger\right) + \sum_k g_k \mu_2 \left(\sigma_{\mathrm{B}}^+ a_k + \sigma_{\mathrm{B}}^- a_k^\dagger\right), \tag{10}$$

where σ_j^+ and σ_j^- are the raising and lowering operator for the jth qubit. $g_k\mu_i$ is the coupling strength between qubits and kth mode of the cavity, where μ_i is a dimensionless real parameter. The relative interaction strength and the collective coupling are $r_i = \mu_i/\mu_T$ and $\mu_T = (\mu_1^2 + \mu_2^2)^{1/2}$, respectively. The dimensionless function $\mathscr{F}(t)$ in Eq. (8) is given by

$$\mathscr{F}(t) = \begin{cases} 1 & t \in [0, \tau), \\ 0 & \text{elsewhere}, \end{cases} \tag{11}$$

which is used to switch interactions on or off, and τ is the charging time of the QB. It is assumed that for $t < 0$, charger and QB do not interact with reservoir, while when $t = 0$, charger and battery start their interaction with the reservoir by switching on H_{AE} and H_{BE}, respectively. In this scenario, the charger and QB do not interact with each other. Given that $[H_B + H_E, H_{BE}] \neq 0$, and assuming the environment is in its ground state at $t = 0$, it is plausible that the final energy of the quantum battery (QB) is not solely derived from the charger A. Furthermore, the thermodynamic work involved in modulating the interactions at specific switching times may contribute to the final energy of the QB. Therefore, within the time interval $[0, \tau)$, a fraction of the energy from the charger is transferred to the quantum battery (QB) through the interaction facilitated by the environment. At the final time, τ, the charger and the quantum battery (QB) are once again isolated by severing the connections between A and E and between B and E. It is important to note that in our model, there is no direct interaction between the charger and the quantum battery (QB). Consequently, we investigate a wireless charging mechanism for the QB, wherein the environment acts as an intermediary in the charging process. Subsequently, we will analyze the process of charging and work extraction in the considered model based on the introduced Hamiltonian. The local unitary transformation of the following form will be considered as[74]

$$\begin{aligned} \hat{U} &= \vec{T} \exp\left[-i \int_0^t \left(\hat{H}_{\mathrm{S}}(\tau) + \hat{H}_{\mathrm{E}}(\tau)\right) d\tau\right] \\ &= \exp\left[-i \left\{ \frac{1}{2} \left[\omega_B t + (d_B/\Omega_B) \sin(\Omega_B t)\right] \hat{\sigma}_z^{(B)} \right.\right. \\ &\quad \left.\left. + \frac{1}{2} \left[\omega_A t + (d_A/\Omega_A) \sin(\Omega_A t)\right] \hat{\sigma}_z^{(A)} + \sum_k \omega_k \hat{a}_k^\dagger \hat{a}_k t \right\}\right] \end{aligned} \tag{12}$$

where $\vec{T}$ is the time-ordering operator. So, the effective Hamiltonian can be obtained as

$$H_{eff} = \sum_{j,k} \left(\mu_j \sigma_j^+ g_k a_k e^{-i(\omega_k - \omega_j)t} e^{i(d_j/\Omega_j)\sin\Omega_j t} + H.c.\right). \tag{13}$$

To obtain the above effective Hamiltonian, we have used $H_{eff} = U^\dagger H U + i(\partial U^\dagger/\partial t)U$. Utilizing the Jacobi-Anger expansion, the exponential terms in Eq. (13) can be expressed as

$$e^{\pm i(d_j/\Omega_j)\sin\Omega_j t} = J_0\left(\frac{d_j}{\Omega_j}\right) + 2\sum_{n=1}^{\infty} (\pm i)^n J_n\left(\frac{d_j}{\Omega_j}\right) \cos(n\Omega_j t), \tag{14}$$

in which $J_n\left(\frac{d_j}{\Omega_j}\right)$ is the n-th Bessel function of the first kind. Let us examine the initial state, which is expressed in the following form

$$|\psi_0\rangle = \left(c_{01}|e_A, g_B\rangle + c_{02}|g_A, e_B\rangle\right)|0\rangle_E \tag{15}$$

where $|0\rangle_E$ is the multi-mode vacuum state and c_{0i} $(i = 1, 2)$ are the probability amplitudes. Equation (15) indicates no excitations in the cavity modes, and the qubits are entangled. The state of the system at time t can be derived as

$$\begin{aligned} |\psi(t)\rangle &= c_1(t)|e_A, g_B\rangle|0\rangle_E + c_2(t)|g_A, e_B\rangle|0\rangle_E \\ &\quad + \sum_k c_k(t)|g_A, g_B\rangle\,|1_k\rangle_E, \end{aligned} \tag{16}$$

Here, $|1_k\rangle_E$ denotes the state of the cavity with a single excitation in the k-th mode and $c_{1,2}(t)$ refers to the time-dependent probability amplitude of the relevant quantum state during the evolution governed by the system's Hamiltonian. By substituting Eq. (16) into the Schrödinger equation $i\frac{d}{dt}|\psi(t)\rangle = H_{eff}|\psi(t)\rangle$ and performing the required algebraic manipulations, we derive the following integro-differential equations.

$$\begin{aligned}\dot{c}_1(t) = &-\sum_k \int_0^t |g_k|^2 \ \mathrm{d}t' \Big(\mu_1^2 e^{id_B/\Omega_B\left(\sin(\Omega_B t)-\sin\left(\Omega_B t'\right)\right)} e^{i\delta_k^{(B)}\left(t-t'\right)} c_1\left(t'\right) \\ &+\mu_1\mu_2 e^{id_B/\Omega_B \sin(\Omega_B t)} e^{-id_A/\Omega_A \sin\left(\Omega_A t'\right)} e^{i\delta_k^{(B)} t} e^{-i\delta_k^{(A)} t'} c_2\left(t'\right)\Big), \\ \dot{c}_2(t) = &-\sum_k \int_0^t |g_k|^2 \ \mathrm{d}t' \Big(\mu_2^2 e^{id_A/\Omega_A\left(\sin(\Omega_A t)-\sin\left(\Omega_A t'\right)\right)} e^{i\delta_k^{(A)}\left(t-t'\right)} c_2\left(t'\right) \\ &+\mu_1\mu_2 e^{-id_B/\Omega_B \sin\left(\Omega_B t'\right)} e^{id_A/\Omega_A \sin(\Omega_A t)} e^{-i\delta_k^{(B)} t'} e^{i\delta_k^{(A)} t} c_1\left(t'\right)\Big).\end{aligned} \tag{17}$$

where $\delta_k^{(j)} = \omega_k - \omega_j$. When considering the continuous spectrum of the environment frequencies, we transition from summation over modes to integration using the following relation: $\sum_k |g_k|^2 \to \int d\omega J(\omega)$, where $J(\omega) = W^2\lambda/\pi[(\omega-\omega_c)^2+\lambda^2]$ is the Lorentzian spectral density with ω_c is the fundamental frequency of the cavity. In this context, W is proportional to the vacuum Rabi frequency ($\mathscr{R} = \mu_T W$), and λ represents the cavity losses (the rate at which the photons escape the cavity). To characterize the coupling strength, we introduce the dimensionless ratio $R = \mathscr{R}/\lambda$. This ratio serves as a criterion for identifying the coupling regime: the system is in the strong coupling limit when $R >> 1$ and the weak coupling limit when $R << 1$.

By defining the correlation function as $f(t,t') = \int d\omega J(\omega) e^{i(\omega_c-\omega)(t-t')}$, Eq. (17) transform into the following form

$$\begin{aligned}\dot{c}_1(t) = &-\int_0^t \mathrm{d}t' f\left(t,t'\right) \Big(\mu_1^2 e^{id_B/\Omega_B\left(\sin(\Omega_B t)-\sin\left(\Omega_B t'\right)\right)} c_1\left(t'\right) \\ &+\mu_1\mu_2 e^{id_B/\Omega_B \sin(\Omega_B t)} e^{-id_A/\Omega_A \sin\left(\Omega_A t'\right)} e^{-i\delta_{AB} t'} c_2\left(t'\right)\Big) e^{i\delta_B\left(t-t'\right)}, \\ \dot{c}_2(t) = &-\int_0^t \mathrm{d}t' f\left(t,t'\right) \Big(\mu_1\mu_2 e^{-id_B/\Omega_B \sin\left(\Omega_B t'\right)} e^{id_A/\Omega_A \sin(\Omega_A t)} e^{i\delta_{AB} t'} c_1\left(t'\right) \\ &+\mu_2^2 e^{id_A/\Omega_A\left(\sin(\Omega_A t)-\sin\left(\Omega_A t'\right)\right)} c_2\left(t'\right)\Big) e^{i\delta_A\left(t-t'\right)},\end{aligned} \tag{18}$$

where $\delta_j = \omega_j - \omega_c$ and $\delta_{AB} = \omega_A - \omega_B$. Consider the special case where the two qubits are identical, such that $\omega_B = \omega_A \equiv \omega_0$, $\Omega_B = \Omega_A \equiv \Omega$ and $d_B = d_A \equiv d$. So, we have $\delta_A = \delta_B \equiv \delta$ and $\delta_{AB} = 0$. Considering these situations Eq. (18) reduces to

$$\begin{aligned}\dot{c}_1(t) &= -\int_0^t \mathrm{d}t' F\left(t,t'\right)\left(\mu_1^2 c_1\left(t'\right) + \mu_1\mu_2 c_2\left(t'\right)\right), \\ \dot{c}_2(t) &= -\int_0^t \mathrm{d}t' F\left(t,t'\right)\left(\mu_2^2 c_2\left(t'\right) + \mu_1\mu_2 c_1\left(t'\right)\right),\end{aligned} \tag{19}$$

where $F(t,t') = W^2 e^{(-\lambda+i\delta)(t-t')} e^{id/\Omega(\sin(\Omega t)-\sin(\Omega t'))}$.

We set $\dot{c}_i = 0$ in Eq. (19) to achieve a stable entangled state. This produces the following long-lived, decoherence-free state

$$|\psi_-\rangle = r_2|e_A, g_B\rangle - r_1|g_B, e_A\rangle, \tag{20}$$

where r_1 and r_2 are the probability amplitudes. $|\psi_-\rangle$ is a subradiant, decoherence-free eigenstate of Hamiltonian 8, exhibiting no temporal decay. Such states arise when both atoms possess identical Bohr frequencies. The state in Eq. (20) experiences no decoherence or change over time. Since $|\psi_-\rangle$ remains static, the only observable time evolution is that of its orthogonal state $|\psi_+\rangle = r_1|e_A, g_B\rangle + r_2|g_A, e_B\rangle$. The survival amplitude of the above state can be described as $\mathscr{E}(t) = \langle\psi_+|\psi_+(t)\rangle$. The survival amplitude is governed by the following integro-differential equation of motion

$$\dot{\mathscr{E}}(t) = \mu_T^2 \int_0^t F(t,t')\mathscr{E}(t')dt'. \tag{21}$$

so, the time-dependent probability amplitude in Eq. (16) can be derived as follows

$$\begin{aligned}c_1(t) &= \left[r_2^2 + r_1^2\mathscr{E}(t)\right] c_{01} - r_1 r_2[1-\mathscr{E}(t)]c_{02}, \\ c_2(t) &= -r_1 r_2[1-\mathscr{E}(t)]c_{01} + \left[r_1^2 + r_2^2\mathscr{E}(t)\right] c_{02}.\end{aligned} \tag{22}$$

Results and discussion

This section provides a comprehensive analysis of each step involved in the quantum battery (QB) charging process within the specified model. By performing a partial trace over each subsystem A and B in Eq. (16), we

can obtain the reduced time-dependent density matrices corresponding to the QB and charger at the specific time $t = \tau$,[3]

$$\begin{aligned}\rho_B(\tau) &= |c_2(\tau)|^2 |e_B\rangle\langle e_B| \left(1 - |c_2(\tau)|^2\right) |g_B\rangle\langle g_B|,\\ \rho_A(\tau) &= |c_1(\tau)|^2 |e_A\rangle\langle e_A| \left(1 - |c_1(\tau)|^2\right) |g_A\rangle\langle g_A|,\end{aligned} \tag{23}$$

To explore the relation between the energy of the QB and the charger, it is beneficial to analyze their respective energy variations. The variation in the internal energy of the QB during the charging process can be expressed as follows:

$$\Delta E_B = Tr\left[H_B \rho_B(\tau)\right] - Tr\left[H_B \rho_B(0)\right], \tag{24}$$

where $H_B = (\omega_0/2)\sigma_z$ is the free Hamiltonian of the QB and $\rho_B(\tau)$ is the state of the QB at time τ. So, the changes in the internal energy of the QB ΔE_B can be derived as

$$\Delta E_B = \omega_0 \left(|c_2(\tau)|^2 - |c_2(0)|^2\right). \tag{25}$$

The maximum work that can be extracted from a quantum battery (QB) at the end of the charging process, when subjected to cyclic unitary operations, is defined as

$$\mathscr{W} = \mathscr{W}_{max} \left(2\,|c_2(\tau)|^2 - 1\right) \Theta\left(|c_2(\tau)|^2 - \frac{1}{2}\right), \tag{26}$$

where $\Theta(x)$ is the Heaviside function and $\mathscr{W}_{max} = \omega_0$ (For more details see Ref.[3]).

Our initial assumption is that the quantum battery (QB) is entirely devoid of energy, while the charger contains significantly more internal energy than the QB. This scenario arises when the state of the composite quantum system encompassing the quantum battery (QB), the charger, and the environment can be described as follows:

$$|\psi_o\rangle = |e\rangle_A |g\rangle_B \otimes |0\rangle_E, \quad (c_{01} = 1, c_{02} = 0). \tag{27}$$

We begin the quantitative analysis by studying the time evolution of the energy change of the QB (ΔE_B) under a strong coupling regime ($R = 5\lambda$), plotted in Fig. 2 for different values of the modulation frequency (Ω) and fixed modulation amplitude $d = 10\lambda$. This evolution is compared to the situation without a modulation process ($d = 0, \Omega = 0$). In this case, fluctuations disappear around time $\lambda\tau \sim 10$. Frequent modulation improves the energy dynamics of the quantum battery for $\Omega \leq 1$. Namely, low-frequency modulation delays the process of reaching a steady state. On the other hand, the energy variation of the quantum battery (QB) decreases as the modulation frequency increases (Fig. 2b). The mechanism behind this is related to the fact that when the modulation frequency becomes large, the system dynamics lose their ability to synchronize effectively with the driving modulation. Instead, the rapid oscillations induced by this high-frequency modulation tend to cancel each other over time. As a result, the energy exchange between the QB and its surrounding environment is significantly reduced. This effect, known as "dynamical decoupling," occurs because the system struggles to absorb or transfer energy when the modulation frequency goes beyond a certain limit. As a result, the energy change in the QB decreases as the modulation frequency increases in this high-frequency range.

Figure 3 displays the ergotropy versus the scaled time parameter $\lambda\tau$ for various modulation frequencies. Other parameters are taken as in Fig. 2. It is seen that the ergotropy can be significantly affected by frequency modulation. For $\Omega \leq 1$, both the amount of work that can be extracted from the system and the time interval for extracting this work increase compared to the off-modulation scenario. Conversely, as Ω increases after $\Omega = 1$, the amount of work that can be extracted and the required time interval decrease. This results in a disruption of the system's coherence, and the quantum correlations that are necessary for efficient work extraction are weakened. As a consequence, the system is unable to reach a state of optimal energy alignment for work extraction, leading to a decrease or destruction of the ergotropy.

We now aim to examine how variations in modulation amplitude impact the time evolution of ΔE_B and ergotropy, as illustrated in Figs. 4 and 5, respectively. Both columns of Fig. 4 indicate that a decrease in modulation frequency substantially prolongs the duration of ΔE_B oscillations. This finding aligns with the results presented in Fig. 2. Specifically, an increase in modulation frequency acts as a disruptive factor, further diminishing energy variations. Furthermore, by comparing the curves in the two columns of Fig. 4 with those depicted in Fig. 2, we observe that for a fixed modulation frequency, an increase in modulation amplitude not only lengthens the duration of the oscillations but also enhances their amplitude.

In Fig. 5, it is clear that an increase in modulation amplitude considerably enhances the ergotropy of the system. A comparison of the blue solid line in Fig. 3 with the curves shown in Fig. 5 highlights the crucial role of modulation in boosting ergotropy. In such a way, increasing the modulation amplitude while simultaneously reducing the modulation frequency leads to a substantial rise in the amount of work that can be extracted and extending the time intervals available for work extraction.

In Fig. 6, we turn to the weak coupling regime, where the time evolution of ΔE_B [(a), (b)] and $\mathscr{W}/\mathscr{W}_{\max}$ [(c), (d)] is plotted for different modulation frequencies with $R = 0.1\lambda$. Here, the solid-blue line in Fig. 6a, c denotes the scenario in which modulation is turned off ($\Omega = 0$ and $d = 0$). It is seen that, in the absence of modulation, the energy change of QB reaches a steady-state value from a starting point of zero without any oscillation, resulting in zero ergotropy. However, when modulation is applied, especially at low frequencies,

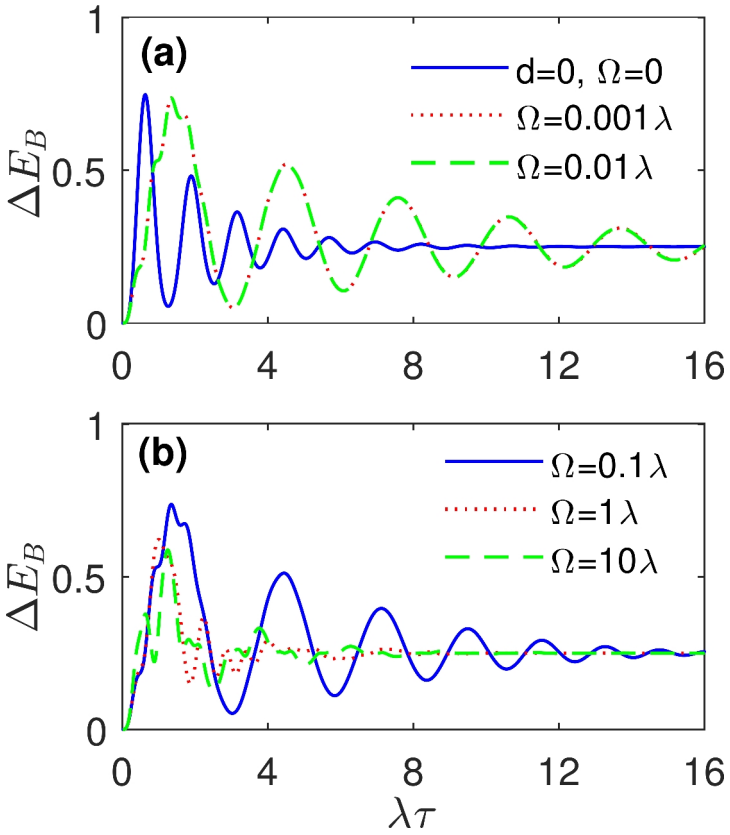

Fig. 2. The energy change of QB (ΔE_B) as a function of scaled time $\lambda\tau$ for different values of the modulation frequency Ω in the strong coupling regime with $R = 5\lambda$. The values of other parameters are: $d = 10\lambda$ and $r_1 = r_2 = 1/\sqrt{2}$. Solid-blue line in panel (**a**) corresponds to the situation in which frequency modulation is off.

oscillations emerge in the dynamic behaviour of ΔE_B, enabling work extraction from the system. Therefore, oscillations of ΔE_B increase as the modulation frequency decreases, leading to a greater capacity for work extraction. Conversely, as the modulation frequency rises, the oscillations of ΔE_B and the associated ergotropy diminish. Figure 6 presents an intriguing result, demonstrating that work can be extracted from the system via modulation, even in the weak coupling regime. However, this phenomenon occurs at very low frequencies.

Finally, it is important to note that our calculations indicate that adjusting the ratio of the amplitude and frequency of modulation at the zeros of the Bessel function of various orders-by changing the modulation frequency-will not yield better results than the situation in which the modulation is off.

Experimental feasibility

Recent advancements in circuit quantum electrodynamics (CQED) and qubit control technologies have made the proposed model experimentally feasible using current superconducting qubit technologies[79–84]. This model leverages well-established frequency modulation techniques. Figure 7 illustrates a schematic diagram of the model within the CQED setup. In this configuration, two flux-tunable transmon qubits-referred to as Qubit A (the charger) and Qubit B (the battery)-are coupled to a shared coplanar waveguide (CPW) resonator, which serves as a structured environment. The resonator facilitates energy transfer between the qubits without direct interaction. Both qubits can couple with different capacitive or inductive strengths to allow different μ_1 and μ_2 . Each qubit is equipped with a dedicated DC flux line for static tuning of the transition frequency (denoted as ω_{0_j} and an AC flux line for sinusoidal modulation, expressed as $d_j \cos(\Omega_j t)$. A typical transition frequency for such a qubit ranges from $\omega_0 \approx 4 - 6.5$ GHz, with a decay rate of approximately $\gamma \approx 5 - 50$ kHz and a size of about $l \approx 100\ \mu$ m. The modulation frequency Ω_j is expected to be between 100 kHz and 10 MHz, while the modulation amplitude d_j will be around 10 MHz. Additionally, a readout resonator connected to a Josephson Parametric Amplifier (JPA) enables high-fidelity measurement of the qubit states. This setup aligns with the architecture seen in many superconducting qubit experiments (like in Yale, IBM, or Google labs)[85–90].

Conclusion

This work investigated the charging performance of a frequency-modulated quantum battery (QB) embedded in a dissipative cavity environment. By modeling the system as two frequency-modulated qubits coupled to a common zero-temperature reservoir, we explored how modulation parameters influence the charging process and ergotropy under both weak and strong coupling regimes. Our results reveal that frequency modulation

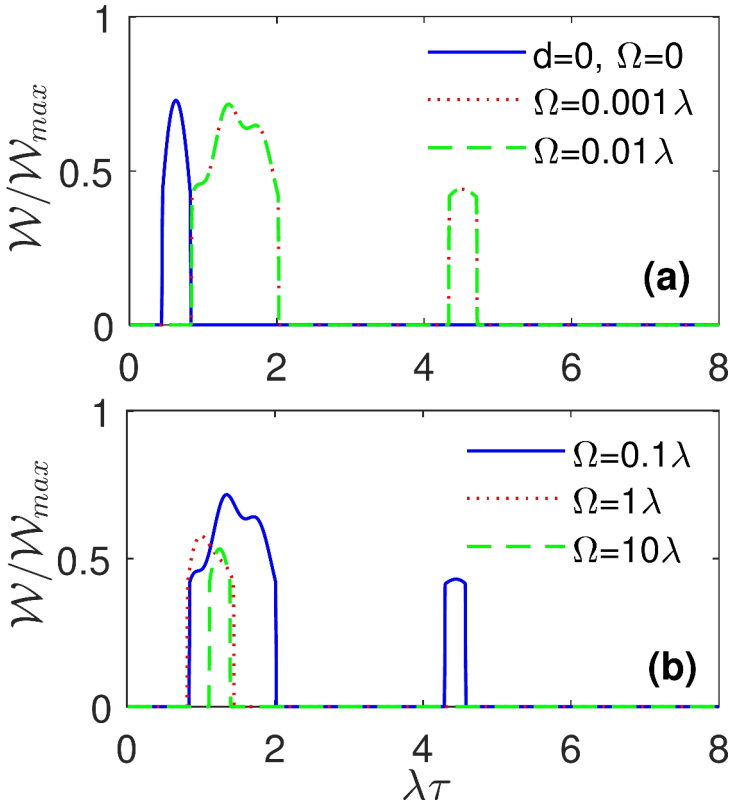

Fig. 3. The dynamics behaviour of $\mathscr{W}/\mathscr{W}_{\max}$ as a function of scaled time $\lambda\tau$. Other parameters are taken as in Fig. 2.

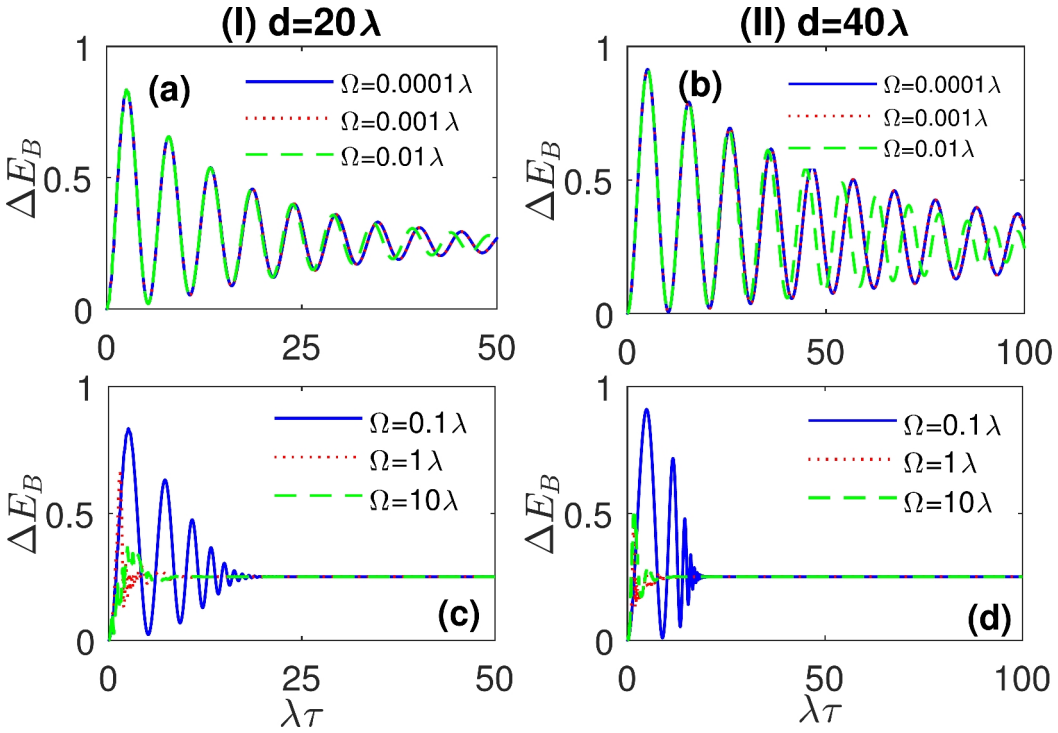

Fig. 4. The energy change of QB (ΔE_B) as a function of scaled time $\lambda\tau$ for different values of the modulation frequency Ω in the strong coupling regime with $R = 5\lambda$. The values of other parameters are: $r_1 = r_2 = 1/\sqrt{2}$, $d = 20$ for column (I) and $d = 40$ for column (II).

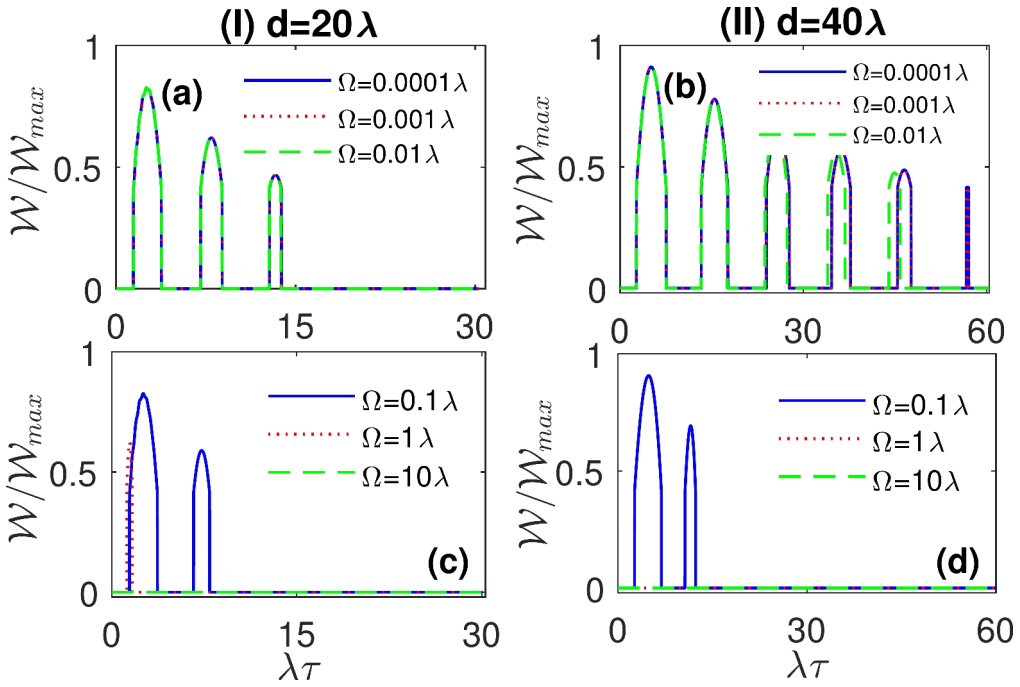

Fig. 5. The dynamics behaviour of $\mathscr{W}/\mathscr{W}_{\max}$ as a function of scaled time $\lambda\tau$ for different values of the modulation frequency Ω. Other parameters are taken as in Fig. 4.

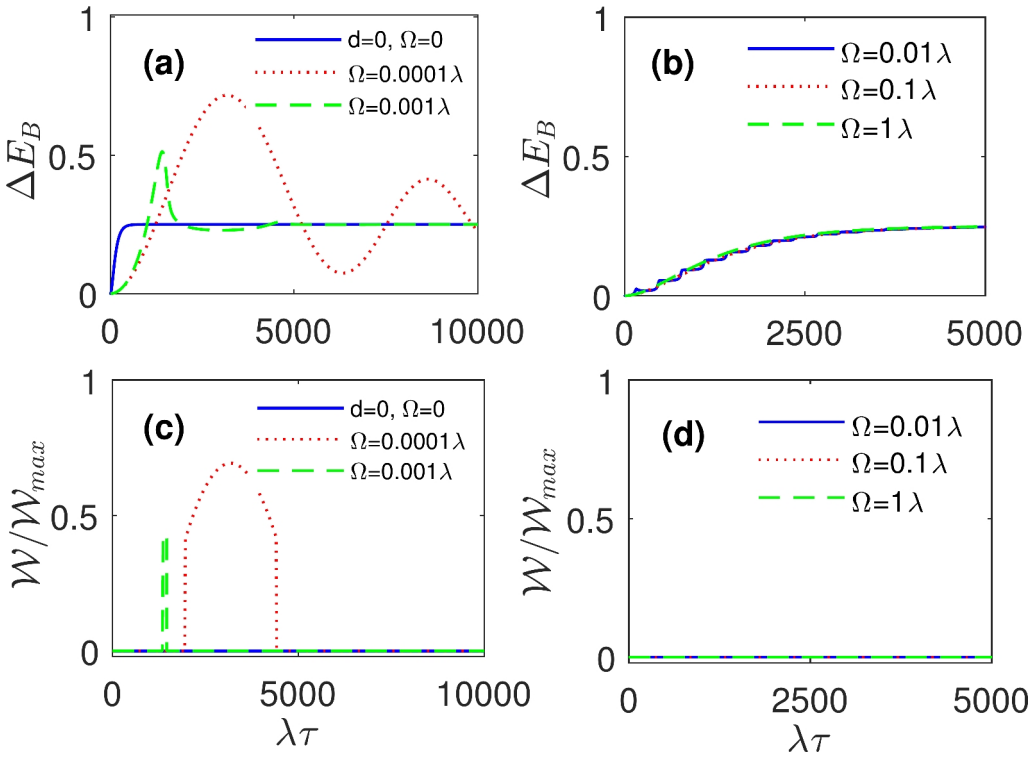

Fig. 6. The dynamics behaviour of ΔE_B (**a** , **b**) and $\mathscr{W}/\mathscr{W}_{\max}$ (**c** , **d**) as functions of scaled time $\lambda\tau$ for different values of the modulation frequency Ω in the weak coupling regime with $R = 0.1\lambda$. The values of other parameters are: $r_1 = r_2 = 1/\sqrt{2}$ and $d = 10\lambda$. Solid-blue line in panels (**a**) and (**b**) corresponds to the situation in which frequency modulation is off.

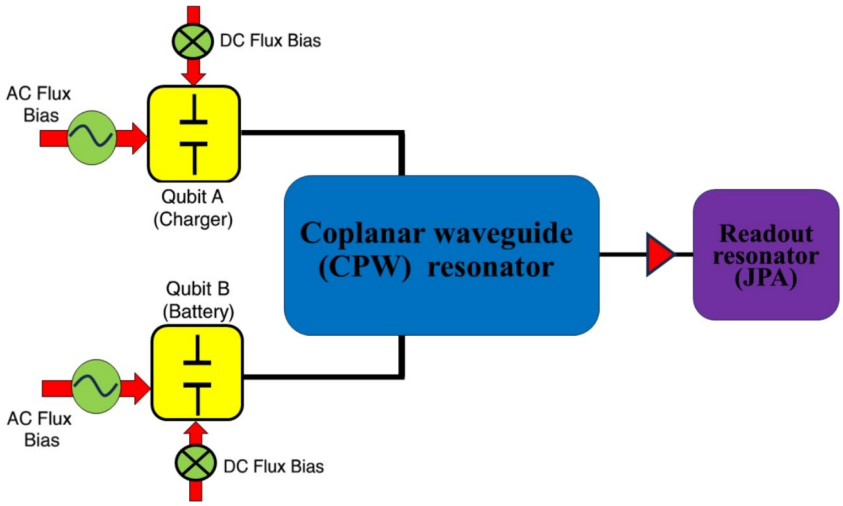

Fig. 7. Schematic diagram of an experimental setup for a frequency-modulated quantum battery using superconducting transmon qubits in a circuit QED architecture. Two flux-tunable transmon qubits-Qubit A (charger) and Qubit B (battery)-are coupled to a shared coplanar waveguide (CPW) resonator acting as a structured environment.

plays a crucial role in optimizing the performance of the quantum battery. In the strong coupling regime, we found that high-amplitude, low-frequency modulation significantly enhances both the charging efficiency and the extractable work. However, the charging performance degrades for higher modulation frequencies due to disruptive effects on energy transfer and coherence. A particularly noteworthy result emerged in the weak coupling regime: while work extraction is typically infeasible in this regime, we demonstrated that applying very low-frequency modulation enables energy storage and work extraction. This effect is otherwise impossible without modulation. This finding is of fundamental importance, as it suggests that even under weak coupling conditions, the strategic use of frequency modulation can transform an inefficient quantum battery into a functional and extractable energy resource. Overall, our findings underscore the importance of modulation as a powerful tool for enhancing quantum battery performance. By carefully tuning the modulation parameters, one can significantly improve charging efficiency and ergotropy, even in regimes where work extraction was previously considered unachievable. These insights pave the way for practical implementations of quantum batteries in real-world quantum technologies, offering a new avenue for efficient energy storage and management in quantum systems. We believe that frequency modulation could effectively enhance the performance of such quantum batteries, even at low temperatures. The main results of this study hold in finite-temperature environments. However, since temperature is a source of decoherence, the absolute zero (zero-temperature) results will outperform those obtained at higher temperatures, including low temperatures. It is worth noting that considering temperature will complicate the calculations significantly. We have already considered this idea and plan to implement it in the future.

Data availability

Data sets generated during the current study are available from the corresponding author on reasonable request.

Received: 7 February 2025; Accepted: 18 April 2025
Published online: 25 April 2025

References

1. Breuer, H.-P. & Petruccione, F. *The Theory of Open Quantum Systems* (Oxford University Press/Cambridge University Press, 2007).
2. Joshi, J. & Mahesh, T. S. Experimental investigation of a quantum battery using star-topology NMR spin systems. *Phys. Rev. A* **106**, 042601 (2022).
3. Tabesh, F. T., Kamin, F. H. & Salimi, S. Environment-mediated charging process of quantum batteries. *Phys. Rev. A* **102**(5), 052223 (2020).
4. Kamin, F. H., Abuali, Z., Ness, H. & Salimi, S. Quantum battery charging by non-equilibrium steady-state currents. *J. Phys. A Math Theor.* **56**(27), 275302 (2023).
5. Kamin, F. H., Salimi, S. & Arjmandi, M. B. Steady-state charging of quantum batteries via dissipative ancillas. *Phys. Rev. A* **109**(2), 022226 (2024).
6. Hadipour, M., Haseli, S., Wang, D. & Haddadi, S. Proposed scheme for a cavity-based quantum battery. *Adv. Quantum Technol.* **7**(11), 2400115 (2024).
7. Hadipour, M. & Haseli, S. Enhancing the efficiency of open quantum batteries via adjusting the classical driving field. *Results Phys.* **64**, 107928 (2024).
8. Hadipour, M. & Haseli, S. Extracting work from two gravitational cat states. *EPL* **147**, 29003 (2024).
9. Hadipour, M. & Haseli, S. Work extraction from quantum coherence in non-equilibrium environment. *Sci. Rep.* **14**(1), 24876 (2024).

10. Hadipour, M. & Haseli, S. Steady-state work extraction from two coupled qubits embedded within equilibrium and non-equilibrium reservoirs. arXiv preprint arXiv:2406.09580
11. Zhu, G., Chen, Y., Hasegawa, Y. & Xue, P. Charging quantum batteries via indefinite causal order: Theory and experiment. *Phys. Rev. Lett.* **131**, 240401 (2023).
12. Andolina, G. M. et al. Charger-mediated energy transfer in exactly solvable models for quantum batteries. *Phys. Rev. B* **98**, 205423 (2018).
13. Le, T. P., Levinsen, J., Modi, K., Parish, M. M. & Pollock, F. A. Spin-chain model of a many-body quantum battery. *Phys. Rev. A* **97**, 022106 (2018).
14. Zhang, Y.-Y., Yang, T.-R., Fu, L. & Wang, X. Powerful harmonic charging in a quantum battery. *Phys. Rev. E* **99**, 052106 (2019).
15. Barra, F. Dissipative charging of a quantum battery. *Phys. Rev. Lett.* **122**, 210601 (2019).
16. Santos, A. C., Cakmak, B., Campbell, S. & Zinner, N. T. Stable adiabatic quantum batteries. *Phys. Rev. E* **100**, 032107 (2019).
17. Andolina, G. M. et al. Extractable work, the role of correlations, and asymptotic freedom in quantum batterie. *Phys. Rev. Lett.* **122**, 047702 (2019).
18. Crescente, A., Carrega, M., Sassetti, M. & Ferraro, D. Ultrafast charging in a two-photon Dicke quantum battery. *Phys. Rev. B* **102**, 245407 (2020).
19. Santos, A. C., Saguia, A. & Sarandy, M. S. Stable and charge-switchable quantum batteries. *Phys. Rev. E* **101**, 062114 (2020).
20. Santos, A. C. Quantum advantage of two-level batteries in the self-discharging process. *Phys. Rev. E* **103**, 042118 (2021).
21. Ghosh, S., Chanda, T., Mal, S. & Sen(De), A. Fast charging of a quantum battery assisted by noise. *Phys. Rev. A***104**, 032207 (2021).
22. Delmonte, A., Crescente, A., Carrega, M., Ferraro, D. & Sassetti, M. Characterization of a two-photon quantum battery: Initial conditions, stability and work extraction. *Entropy* **23**, 612 (2021).
23. Li, J. L., Shen, H. Z. & Yi, X. X. Quantum batteries in non-Markovian reservoirs. *Opt. Lett.* **47**, 5614 (2022).
24. Dou, F.-Q., Lu, Y.-Q., Wang, Y.-J. & Sun, J.-A. Extended Dicke quantum battery with interatomic interactions and driving field. *Phys. Rev. B* **105**, 115405 (2022).
25. Barra, F., Hovhannisyan, K. V. & Imparato, A. Quantum batteries at the verge of a phase transition. *New J. Phys.* **24**, 015003 (2022).
26. Carrasco, J., Maze, J. R., Hermann-Avigliano, C. & Barra, F. Collective enhancement in dissipative quantum batteries. *Phys. Rev. E* **105**, 064119 (2022).
27. Shaghaghi, V., Singh, V., Benenti, G. & Rosa, D. Micromasers as quantum batteries. *Quantum Sci. Technol.***7**, 04LT01 (2022).
28. Rodriguez, C., Rosa, D. & Olle, J. Artificial intelligence discovery of a charging protocol in a micromaser quantum battery. *Phys. Rev. A* **108**, 042618 (2023).
29. Santos, T. F. F., de Almeida, Y. V. & Santos, M. F. Vacuum-enhanced charging of a quantum battery. *Phys. Rev. A* **107**, 032203 (2023).
30. Downing, C. A. & Ukhtary, M. S. A quantum battery with quadratic driving. *Commun. Phys.* **6**, 322 (2023).
31. Gemme, G., Andolina, G. M., Pellegrino, F. M. D., Sassetti, M. & Ferraro, D. Off-resonant Dicke quantum battery: charging by virtual photons. *Batteries* **9**, 197 (2023).
32. Shaghaghi, V., Singh, V., Carrega, M., Rosa, D. & Benenti, G. Lossy micromaser battery: Almost pure states in the Jaynes–Cummings regime. *Entropy* **25**, 430 (2023).
33. Dou, F.-Q. & Yang, F.-M. Superconducting transmon qubit-resonator quantum battery. *Phys. Rev. A* **107**, 023725 (2023).
34. Gumberidze, M., Kolar, M. & Filip, R. Measurement induced synthesis of coherent quantum batteries. *Sci. Rep.* **9**, 19628 (2019).
35. Kamin, F. H., Tabesh, F. T., Salimi, S. & Santos, A. C. Entanglement, coherence, and charging process of quantum batteries. *Phys. Rev. E* **102**, 052109 (2020).
36. Shi, H.-L., Ding, S., Wan, Q.-K., Wang, X.-H. & Yang, W.-L. Entanglement, coherence, and extractable work in quantum batteries. *Phys. Rev. Lett.* **129**, 130602 (2022).
37. Arjmandi, M. B., Shokri, A., Faizi, E. & Mohammadi, H. Performance of quantum batteries with correlated and uncorrelated chargers. *Phys. Rev. A* **106**, 062609 (2022).
38. Arjmandi, M. B., Mohammadi, H., Saguia, A., Sarandy, M. S. & Santos, A. C. Localization effects in disordered quantum batteries. *Phys. Rev. E* **108**, 064106 (2023).
39. Farina, D., Andolina, G. M., Mari, A., Polini, M. & Giovannetti, V. Charger-mediated energy transfer for quantum batteries: An open-system approach. *Phys. Rev. B* **99**, 035421 (2019).
40. Carrega, M., Crescente, A., Ferraro, D. & Sassetti, M. Dissipative dynamics of an open quantum battery. *New J. Phys.* **22**, 083085 (2020).
41. Kamin, F. H., Tabesh, F. T., Salimi, S., Kheirandish, F. & Santos, A. C. Non-Markovian effects on charging and self-discharging process of quantum batteries. *New J. Phys.* **22**, 083007 (2020).
42. Zakavati, S., Tabesh, F. T. & Salimi, S. Bounds on charging power of open quantum batteries. *Phys. Rev. E* **104**, 054117 (2021).
43. Xu, K., Zhu, H.-J., Zhang, G.-F. & Liu, W.-M. Enhancing the performance of an open quantum battery via environment engineering. *Phys. Rev. E* **104**, 064143 (2021).
44. Arjmandi, M. B., Mohammadi, H. & Santos, A. C. Enhancing self-discharging process with disordered quantum batteries. *Phys. Rev. E* **105**, 054115 (2022).
45. Song, M.-L., Li, L.-J., Song, X.-K., Ye, L. & Wang, D. Environment-mediated entropic uncertainty in charging quantum batteries. *Phys. Rev. E* **106**, 054107 (2022).
46. Hadipour, M., Haseli, S., Dolatkhah, H. & Rashidi, M. Study the charging process of moving quantum batteries inside cavity. *Sci. Rep.* **13**, 10672 (2023).
47. Mojaveri, B., Jafarzadeh Bahrbeig, R., Fasihi, M. A. & Babanzadeh, S. Enhancing the direct charging performance of an open quantum battery by adjusting its velocity. *Sci. Rep.***13**, 19827 (2023).
48. Xu, K., Zhu, H.-J., Zhu, H., Zhang, G.-F. & Liu, W.-M. Charging and self-discharging process of a quantum battery in composite environments. *Front. Phys.* **18**, 31301 (2023).
49. Morrone, D., Rossi, M. A. C., Smirne, A. & Genoni, M. G. Charging a quantum battery in a non-Markovian environment: A collisional model approach. *Quantum Sci. Technol.* **8**, 035007 (2023).
50. Catalano, A. G., Giampaolo, S. M., Morsch, O., Giovannetti, V. & Franchini, F. Frustrating quantum batteries. arXiv:2307.02529 (2023).
51. Mojaveri, B., Bahrbeig, R. J. & Fasihi, M. A. Charging a quantum battery mediated by parity-deformed fields, arXiv preprint arXiv:2405.11356 (2024).
52. Grazi, R., Shaikh, D. S., Sassetti, M., Ziani, N. T. & Ferraro, D. Controlling energy storage crossing quantum phase transitions in an integrable spin quantum battery. *Phys. Rev. Lett.* **133**, 197001 (2024).
53. Gyhm, J.-Y. & Fischer, U. R. Beneficial and detrimental entanglement for quantum battery charging. *AVS Quantum Sci.* **6**, 012001 (2024).
54. Lu, Z.-G., Tian, G., Lu, X.-Y. & Shang, C. Topological quantum batteries.
55. Ferraro, D., Campisi, M., Andolina, G. M., Pellegrini, V. & Polini, M. High-power collective charging of a solid-state quantum battery. *Phys. Rev. Lett.* **120**, 117702 (2018).
56. Ahmadi, B., Mazurek, P., Barzanjeh, S. & Horodecki, P. Cryogenic control architecture for large-scale quantum computing. *Phys. Rev. Appl.* **23**, 024010 (2025).
57. Shaghaghi, V., Singh, V., Benenti, G. & Rosa, D. Micromasers as quantum batteries. *Quantum Sci. Technol.***7**, 04LT01 (2022).
58. Noel, M. W., Griffith, W. M. & Gallagher, T. F. Frequency-modulated excitation of a two-level atom. *Phys. Rev. A* **58**, 2265 (1998).

59. Silveri, M. P., Tuorila, J. A., Thuneberg, E. V. & Thuneberg, G. S. Quantum systems under frequency modulation. *Rep. Prog. Phys.* **80**, 056002 (2017).
60. Trabesinger, A. Quantum computing: Towards reality. *Nature* **543**, S1 (2017).
61. Nakamura, Y., Pashkin, Y. A. & Tsai, J. S. Rabi oscillations in a Josephson–Junction charge two-level system. *Phys. Rev. Lett.* **87**, 246601 (2001).
62. Oliver, W. D. et al. Mach–Zehnder interferometry in a strongly driven superconducting qubit. *Science* **310**, 1653 (2005).
63. Tuorila, J. et al. Stark effect and generalized Bloch–Siegert shift in a strongly driven two-level system. *Phys. Rev. Lett.* **105**, 257003 (2010).
64. Li, J. et al. Motional averaging in a superconducting qubit. *Nat. Commun.* **4**, 1420 (2013).
65. Beaudoin, F., da Silva, M. P., Dutton, Z. & Blais, A. First-order sidebands in circuit QED using qubit frequency modulation. *Phys. Rev. A* **86**, 022305 (2012).
66. Strand, J. D. et al. First-order sideband transitions with flux-driven asymmetric transmon qubits. *Phys. Rev. B* **87**, 220505(R) (2013).
67. Ficek, Z., Seke, J., Soldatov, A. V. & Adam, G. Fluorescence spectrum of a two-level atom driven by a multiple modulated field. *Phys. Rev. A* **64**, 013813 (2001).
68. Janowicz, M., Orłowski, A. & Mostowski, J. V. Spontaneous emission in a Fabry–Perot cavity: Frequency modulation and collective effects modulation. *J. Phys. B At. Mol. Opt. Phys.* **41**, 065501 (2008).
69. Janowicz, M. Non-Markovian decay of an atom coupled to a reservoir: Modification by frequency modulation. *Phys. Rev. A* **61**, 025802 (2000).
70. Zhou, L., Yang, S., Liu, Y. X., Sun, C. P. & Nori, F. Quantum Zeno switch for single-photon coherent transport. *Phys. Rev. A* **80**, 062109 (2009).
71. Deng, C., Orgiazzi, J. L., Shen, F., Ashhab, S. & Lupascu, A. Observation of Floquet states in a strongly driven artificial atom. *Phys. Rev. Lett.* **115**, 133601 (2015).
72. Macovei, M. & Keitel, C. H. Quantum dynamics of a two-level emitter with a modulated transition frequency. *Phys. Rev. A* **90**, 043838 (2014).
73. Poggi, P. M., Lombardo, F. C. & Wisniacki, D. A. Driving-induced amplification of non-Markovianity in open quantum systems evolution. *EPL* **118**, 20005 (2017).
74. Mortezapour, A. & Lo Franco, R. Protecting quantum resources via frequency modulation of qubits in leaky cavities. *Sci. Rep.* **8**, 14304 (2018).
75. Houshmand Almani, A. H., Mortezapour, A. & Nourmandipour, A. Enhancing Quantum Synchronization in a driven qubit system coupled to a structured environment. arXiv preprint arXiv:2405.11356 (2024).
76. Nourmandipour, A. & Mortezapour, A. Frequency-modulated qubits in a dissipative cavity: Entanglement dynamics and protection. *Quantum Inf. Process.* **22**, 254 (2023).
77. Rajabalinia, A. et al. Quantumness and speedup limit of a qubit under transition-frequency modulation. *Phys. Rev. A* **106**, 062431 (2022).
78. Allahverdyan, A. E., Balian, R. & Nieuwenhuizen, Th. M. Maximal work extraction from finite quantum systems. *EPL* **67**, 565 (2004).
79. Paik, H. et al. Observation of high coherence in Josephson junction qubits measured in a three-dimensional circuit QED architecture. *Phys. Rev. Lett.* **107**, 240501 (2011).
80. Slichter, D. H. et al. Measurement-induced qubit state mixing in circuit QED from up-converted dephasing noise. *Phys. Rev. Lett.* **109**, 153601 (2012).
81. Silveri, M. P., Tuorila, J. A., Thuneberg, E. V. & Paraoanu, G. S. Quantum systems under frequency modulation. *Rep. Prog. Phys.* **80**, 056002 (2017).
82. IBM Research. IBM Q achieves quantum volume of 16, a measure of quantum computer performance (2017).
83. Kjaergaard, M. et al. Superconducting qubits: Current state of play. *Annu. Rev. Condens. Matter Phys.* **11**, 369–395 (2020).
84. Place, A. P. et al. New material platform for superconducting transmon qubits with coherence times exceeding 0.3 milliseconds. *Nat. Commun.* **12**, 1779 (2021).
85. Zakavati, S., Tabesh, F. T. & Salimi, S. Observation of high coherence in Josephson junction qubits measured in a three-dimensional circuit QED architecture. *Phys. Rev. Lett.* **107**, 240501 (2011).
86. Slichter, D. H. et al. Measurement-induced qubit state mixing in circuit QED from up-converted. *Rep. Prog. Phys.* **109**, 153601 (2012).
87. Silveri, M. P., Tuorilaand, J. A., Thuneberg, E. V. & Paraoanu, G. S. Quantum systems under frequency modulation. *Rep. Prog. Phys.* **80**, 056002 (2017).
88. https://www-03.ibm.com/press/us/en/pressrelease/53374.wss (2017).
89. Kjaergaard, M. et al. Superconducting qubits: Current state of play. *Annu. Rev. Condens. Matter Phys.* **11**, 369 (2020).
90. Place, A. P. et al. New material platform for superconducting transmon qubits with coherence times exceeding 0.3 milliseconds. *Nat. Commun.* **12**, 1779 (2021).

Acknowledgements

Maryam Hadipour and Soroush Haseli acknowledge the Iran National Science Foundation (INSF) for supporting this work under project No.4039863.

Author contributions

Maryam Hadipour, Negar Nikdel Yousefi, Ali Mortezapour, Amir Sharifi Miavaghi and Soroush Haseli all contributed to the development and completion of the idea, performing the calculations, analyzing the results, discussions and writing the manuscript.

Declarations

Competing interests

The authors declare that they have no known competing financial interests.

Additional information

Correspondence and requests for materials should be addressed to S.H.

Reprints and permissions information is available at www.nature.com/reprints.